Subharmonic wave transition in a quasi-one-dimensional noisy fluidized shallow granular bed

Ignacio Ortega, Marcel G. Clerc, Claudio Falcón, and Nicolás Mujica
Departamento de Física, Facultad de Ciencias Físicas y Matemáticas, Universidad de Chile, Casilla 487-3, Santiago, Chile
(Received 5 November 2009; published 19 April 2010)

We present an experimental and theoretical study of the pattern formation process of standing subharmonic waves in a fluidized quasi-one-dimensional shallow granular bed. The fluidization process is driven by means of a time-periodic air flow, analogous to a tapping type of forcing. Measurements of the amplitude of the critical mode close to the transition are in quite good agreement with those inferred from a universal stochastic amplitude equation. This allows us to determine both the bifurcation point of the deterministic system and the corresponding noise intensity. We also show that the probability density distribution is well described by a generalized Rayleigh distribution, which is the stationary solution of the corresponding Fokker-Planck equation of the universal stochastic amplitude equation that describes our system.

DOI: 10.1103/PhysRevE.81.046208 PACS number(s): 05.45.−a, 45.70.Qj, 05.40.−a, 47.10.Fg

I. INTRODUCTION

In the course of recent decades, much effort has been devoted to the study of the phenomena exhibited by granular matter [1–3]. However, the richness and complexity of the static and dynamical behaviors of granular materials still present a major challenge in physics and in engineering sciences. Special interest has been given to the possibility of observing fluidization in granular materials. To fluidize a granular system, energy must be injected, for example, by mechanical agitation or an up flow of gas strong enough to counter gravity. The later mechanism is used in industry for mixing solid particles with liquids or gases [4]. This system is of prominent technological importance in catalysis of gas-sphere reactors, transport of powders, and combustion of ores to mention a few [4].

A fundamental question that emerges is the characterization of the self-organized dynamics exhibited by these systems, such as the transition of a granular system from a liquid to solid or gaseous state and pattern formation (see the reviews [1,2] and references therein). In particular, the study of mechanisms of bed instabilities is an active research area in the engineering community. Current fluidization studies mainly focus on thick fluidized beds—deep granular beds—where the thickness of the granular bed is composed by a large number of granular layers. On the other hand, there have been only few studies of instabilities in granular beds formed by a small number of layers, defined as shallow beds [5–7]. For instance, in Ref. [7], the phase diagram of a fluidized shallow quasi-two-dimensional bed composed of 150 μm diameter bronze particles is reported. The observed patterns include subharmonic squares and stripes, quasiperiodic patterns, and disordered structures.

The main difference of granular systems with molecular fluids is that, at collisions, grains dissipate kinetic energy into their internal degrees of freedom. Another important difference is that the individual constituents, the grains, are macroscopic, so that their typical energy is many orders of magnitude larger than the thermal excitation energy kT, where k is the Boltzmann constant and T is the temperature of the grains. In spite of these fundamental differences, fluidized granular matter exhibits a variety of phenomena that resemble those of molecular fluids. Yet, the possibility of finding a continuous or macroscopic description of granular flows is still an open question. There are several models with different approximation schemes that produce different hydrodynamic phenomena under certain limited conditions [8–16].

Granular flows are intrinsically noisy because of their relatively small number of constituents compared to their molecular counterparts. Thus, any attempt for defining field variables, such as local density and velocity, should consider the fact that these are fluctuating quantities [17]. In the case of molecular fluids, one of the earliest works in this direction is the study of the effect of the noise at the onset of Bénard convection [18]. It is important to note that in this seminal work, the Swift-Hohenberg model is proposed, which is a prototype model for pattern formation. From a theoretical point of view, a relevant problem is the influence of noise on self-organization phenomena, such as uncontrollable fluctuations that develop in granular flows and patterns. These fluctuations can transform a simple supercritical bifurcation into an imperfect one or they can amend or shift a bifurcation point, destroy an hysteresis region, induce pattern formation, and so forth (see Ref. [19] and references therein). The changes in dynamical systems generated by the effect of noise, in particular multiplicative noise, have also been studied in the context of oscillatory instabilities [20] even in the presence of periodical forcing [21]. In particular, the probability distribution function of the oscillating field and its bifurcation diagram has been characterized. Experimentally, the effects of uncontrollable fluctuations in granular fluids have been analyzed in Ref. [17] for the case of a vertically oscillated quasi-two-dimensional layer of grains below the critical acceleration for the onset of standing waves. Numerical simulations of a noisy Swift-Hohenberg model are contrasted with the experimental observations [17] and molecular-dynamics simulations [22], which show to be in qualitative agreement. However, as result of the universal nature of pattern formation, one expects that at the onset of the spatial supercritical bifurcations, several noisy models describing the appearance of a supercritical pattern will show the same universal features. It is important to note that a spatial supercritical bifurcation is described in a unified manner by the Ginzburg-Landau equation with real coefficients [26]. Hence, methods and tools of qualitative partial differential theory such as amplitude equations, bifurcation theory, and stochastic processes [23–25] become fundamental to

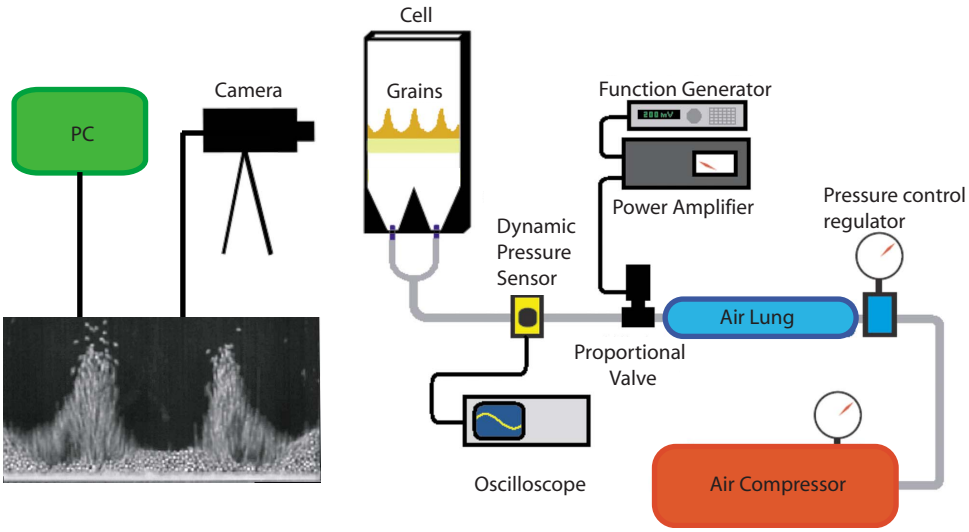

FIG. 1. (Color online) Schematic diagram of the experimental setup. Grains are deposited on top of a porous material inside a quasi-two-dimensional cell. These are fluidized with a periodic air flow. The air flow production and control stages are shown as well as the image acquisition equipment.

grasp the complex and wealthy phenomena exhibited by fluidized granular systems.

Here, we present an experimental and theoretical study of the pattern formation process of standing subharmonic waves in a fluidized quasi-one-dimensional shallow granular bed composed by monodisperse grains. The fluidization process is driven with a time-periodic air flow. We characterize the bifurcation diagram of the standing subharmonic waves. We show that the transition from a flat interface to standing waves is smooth rather than abrupt. This is a direct consequence of noise effects in the pattern dynamics, modifying the deterministic bifurcation curve, such that the critical point and the physical mechanisms are masked by fluctuations [19,26]. The experimental observation of the amplitude of the critical mode is in good agreement with those inferred from a stochastic amplitude equation. In particular, this is applied to the bifurcation curve of the amplitude of standing subharmonic waves. This allows the determination of the bifurcation point, the intensity of pattern fluctuations, and the characterization of the appearance of precursors and patterns. We show that the probability density distribution is described by a generalized Rayleigh distribution, which is the stationary solution of the corresponding Fokker-Planck equation of the universal stochastic amplitude equation.

II. EXPERIMENTAL SETUP

The experimental setup is displayed in Fig. 1. The experimental cell is 45-mm wide, 200-mm tall, and 3.5 mm in depth. The cell is divided it two parts, top and bottom, separated by a thick bandlike porous sponge placed horizontally (2-mm thick, 45-mm wide, and 20-mm tall, Tesa sponge 55604–00007). Approximately 14 000 monodisperse bronze spheres, of diameter $d=350$ μm, are introduced into the cell from above, deposited on top of this horizontal sponge floor. In practice, the mass of grains was used as a control parameter, corresponding to $M=2.8$ g for the results presented in this paper. Typically, the height of deposited grains is about 4 mm. Thus, the granular bed is about $128d$ wide, $6d$ in depth, and $11d$ tall. The grain's sponge floor acts as an homogenization stage, reducing also turbulent fluctuations within the flow.

The granular system is excited by means of a periodic air flow which is generated by an air compressor (Bauker TD4050) and regulated by an electromechanical proportional valve (Teknocraft 203319) via a precision control regulator (Controlair 100) and an air lung. The response time of the valve is less than 4 ms. Its aperture is set by a variable voltage signal controlled by a function generator (Agilent 33250A) through a power amplifier (NF model HFA4011). The proportional valve remains closed for an applied voltage lower than 4 V. Its maximum aperture is obtained at 27 V. For a variable voltage control, the valve presents hysteresis of about 10%. The pressure oscillations induced by the variable air flow are measured before the flow enters the cell with a dynamic pressure sensor (PCB 106B) and an oscilloscope (Tektronix TDS2012B). The two plastic hoses that connect the proportional valve to the dynamic pressure sensor and this sensor to the experimental cell are sufficiently short ($\sim$50 cm) such that the pressure drop between the pressure measurement point and the actual cell air inlet is very small ($<1\%$).

We use a symmetrical triangular signal with a nonzero offset to generate a time-modulated controllable pressure signal. This choice is driven by the motivation of studying the response of a shallow granular bed fluidized by a periodic forcing that is not purely sinusoidal. With our symmetrical triangular signal forcing plus an offset, during a certain period of time of the forcing cycle the proportional valve remains closed, reducing to zero the flow velocity. In vibrofluidized granular systems, this would correspond to a *tapping* type of forcing. In addition, in order to observe fluidization in our current setup with a sinusoidal periodic signal, the offset is so large that grains show mainly a disordered fluidized state.

A typical pressure temporal signal is shown in Fig. 2(a). From this kind of pressure signal, we compute the peak pressure amplitude P_o of the Fourier transform related to the forcing frequency f_o. As we will show later, the most dominant component of the pressure oscillations is related to the forcing frequency f_o. The relation between the applied peak-

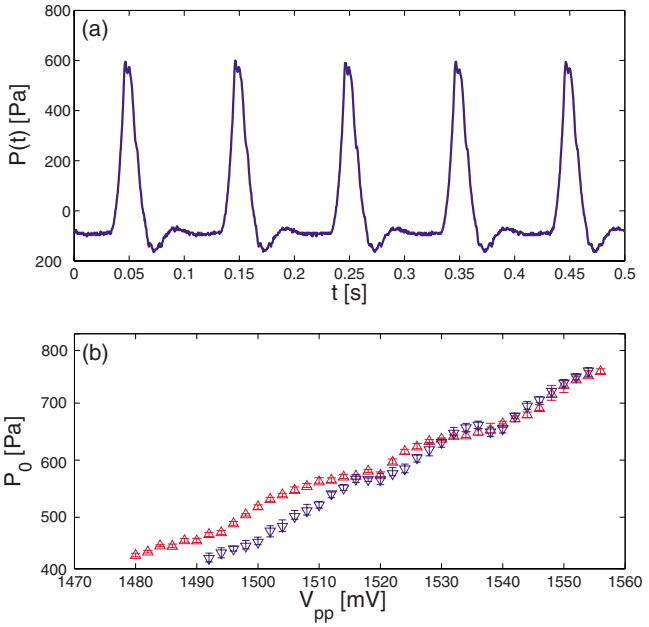

FIG. 2. (Color online) (a) Typical temporal trace of air flow pressure oscillations, which shows the tappinglike forcing. In this case, the peak-to-peak voltage is V_{pp}=1420 mV. (b) Peak pressure amplitude P_o vs V_{pp} obtained for increasing (△) and decreasing (▽) voltage ramps. In this case f_o=10 Hz, the power amplifier gain is 20 and the voltage offset is 200 mV.

peak voltage V_{pp} and P_o is displayed in Fig. 2(b), which is roughly linear. It presents a low level of hysteresis at low-pressure values, consistent with the proportional valve hysteresis reported by its fabricator. For our experimental setup, the control parameters are the forcing frequency f_o and the peak amplitude P_o of the pressure fluctuations at f_o.

The granular bed is illuminated with two high-power halogen lamps and the collective motion of the granular layer is recorded against a black background with a high-speed digital camera (IDT X-Stream X3) at 50 fps during 50 s using a 600×400 pixel^2 window. For each acquired video, its sequence of images and the corresponding pressure signal are processed and analyzed with a desktop computer using MATLAB.

The granular pattern amplitude is calculated by an image-processing method where the granular layer surface profile is obtained for each image. A summary of the main steps is shown in Fig. 3. Examples of raw images, with and without surface waves, are shown in panels (a) and (b). Smoothing is required in order to eliminate single particles that are ejected from the interface which can pollute its correct determination. This smoothing is obtained by filtering the image as shown in figures (c) and (d). After, the granular surface profile $h(x,t)$ is deduced by using an intensity threshold. Examples of such surface profiles are shown with continuous lines in figures (e) and (f). The black background ensures that the profile is well defined for each image, even if the granular bed shows low-density regions beneath its surface.

III. EXPERIMENTAL RESULTS

Increasing P_o for a fixed value of f_o, density fluctuations in the granular layer develop which are related to the small

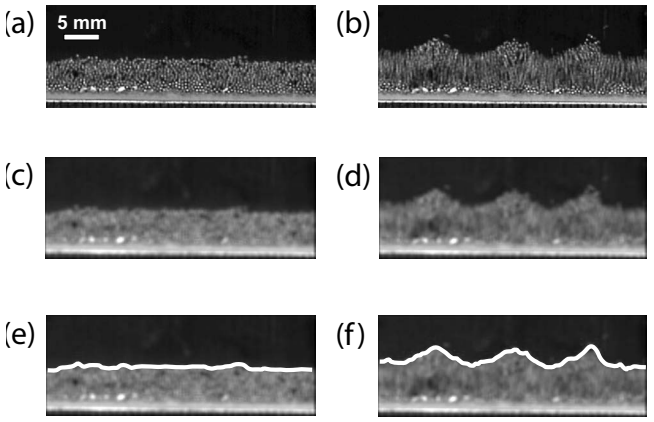

FIG. 3. Image processing method procedure. Left (right) side corresponds to a flat (surface wave) surface, obtained with f_o =10 Hz, P_o=438 Pa (731 Pa). [(a) and (b)] Raw images; [(c) and (d)] neighbor-averaged smoothed images; [(e) and (f)] superposition of surface profile $h(x,t)$, obtained with an intensity threshold.

displacement (less than a diameter) of particles in the bulk. Larger fluctuations are found at the surface of the layer, where fewer collisions occur. As P_o continues to increase, fluctuations of a characteristic wavelength and frequency develop over the surface from time to time, disappearing also randomly with a typical lifetime. This type of fluctuation is commonly known as a *precursor* [27]. In this context, it precedes the appearance of a spatial instability of the flat interface of the granular bed. For larger values of P_o, an oscillating pattern with a fluctuating amplitude appears over the surface of the granular bed oscillating at half the forcing frequency with a wavelength λ_c. Hence, the system develops stationary subharmonic waves through a parametric instability, which is one of the granular counterparts of the well-known subharmonic wave instability in Newtonian fluids, known as the *Faraday instability* [28]. The small amplitude pattern is smooth and can be well fitted by a sinusoidal function. In a frequency band of f_o between 5 and 20 Hz, no distinguishable change in λ_c is observed. This effect is ascribed to the small size of the container under consideration, which discretizes strongly the available wave numbers. For a fixed excitation frequency, there is a smooth transition from the flat interface state to a subharmonic oscillating pattern. The transition value of P_o where the flat interface destabilizes is roughly linear in f_o. In what follows, we will fix the excitation frequency at f_o=10 Hz, which fixes the typical wavelength λ of the pattern at 1.2 cm.

The left panel of Fig. 3 shows that for P_o below a certain threshold value, the fluidized granular bed is flat in average. The right panel of Fig. 3 shows an example of the subharmonic surface waves that appear above the pressure threshold value. As previously noted, the transition between these states is not abrupt. Instead, it is rather smooth. Thus, a good order parameter has to be defined. In order to do so, we now turn to the characterization of the time dependence of the amplitude of the critical mode and the evolution of its envelope.

For each image, the surface-profile curve $h(x,t)$ is numerically Fourier transformed to find the critical wave num-

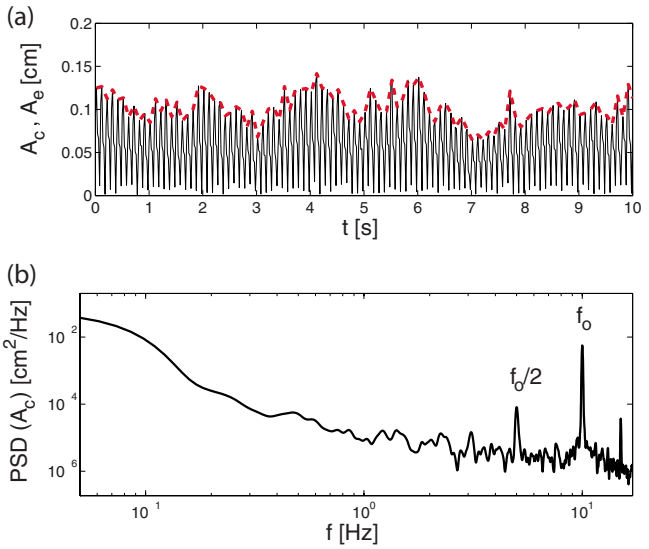

FIG. 4. (Color online) (a) Temporal trace of the fluctuating critical amplitude A_c (continuous line) and its envelope A_e (dashed line) for P_o=655 Pa in a 10 s time window. (b) PSD of the fluctuating critical amplitude A_c.

ber k_c related to the critical wavelength λ_c of the pattern. The average critical wave number over the image sequence is then used to compute the amplitude of the critical mode A_c of the granular pattern for each image. This quantity oscillates with time because of the surface wave subharmonic nature. In addition, due to the intrinsic noisy character of this fluidized granular system, the envelope of critical mode A_c is also a temporally fluctuating quantity.

To illustrate this behavior, a temporal trace of the critical amplitude A_c and its envelope A_e is displayed in Fig. 4(a). There is a strong harmonic oscillation and also slow modulations of amplitude associated to large-scale modulations and inherent fluctuations of the granular bed. From the temporal trace, we compute its power spectrum density (PSD), which is shown in Fig. 4(b). Due to the global motion of the granular bed at f_o, there as a large resonance peak at the harmonic frequency. Also, there is resonance peak at $f_o/2$, which shows the subharmonic character of the spatial instability. For lower frequencies, large amplitude fluctuations develop which are related to the large scale fluctuations of the pattern.

The first cumulants of A_e, i.e., its mean value $\langle A_e \rangle$ and standard deviation $\sigma_{A_e} \equiv \sqrt{\langle A_e^2 \rangle - \langle A_e \rangle^2}$, are computed from the temporal trace of the envelope of the critical amplitude. Figure 5 shows the typical bifurcation diagram for A_e for increasing and decreasing ramps of P_o, where symbols stand for $\langle A_e \rangle$ and error bars for σ_{A_e}. The amplitude of the subharmonic pattern grows smoothly from almost zero, which is related to the minimal discretization of the pattern (the particle radius). No abrupt change is evident, so no critical value of P_o is found for this transition. Hysteresis is not observed between increasing and decreasing P_o ramps. There is also no significant change in the critical wave number k_c of the pattern. It should be noticed that this type of bifurcation diagram has been found in experiments using glass particles [29].

The following theoretical discussion will shed light into why this transition is rather smooth. In summary, the inherent noise present in the fluidized granular bed changes the qualitative form of the bifurcation diagram. By fitting the experimental data with a modified expression, both noise intensity and the bifurcation point of the deterministic system can be obtained. None of them changes between increasing and decreasing P_o ramps. In Fig. 5, the continuous lines correspond to fits of our theoretical prediction that includes effects of noise (see Sec. IV). The dashed lines correspond to the deterministic bifurcation diagram obtained from a theoretical prediction without noise, $\langle A_e \rangle = \alpha_s \varepsilon$, where

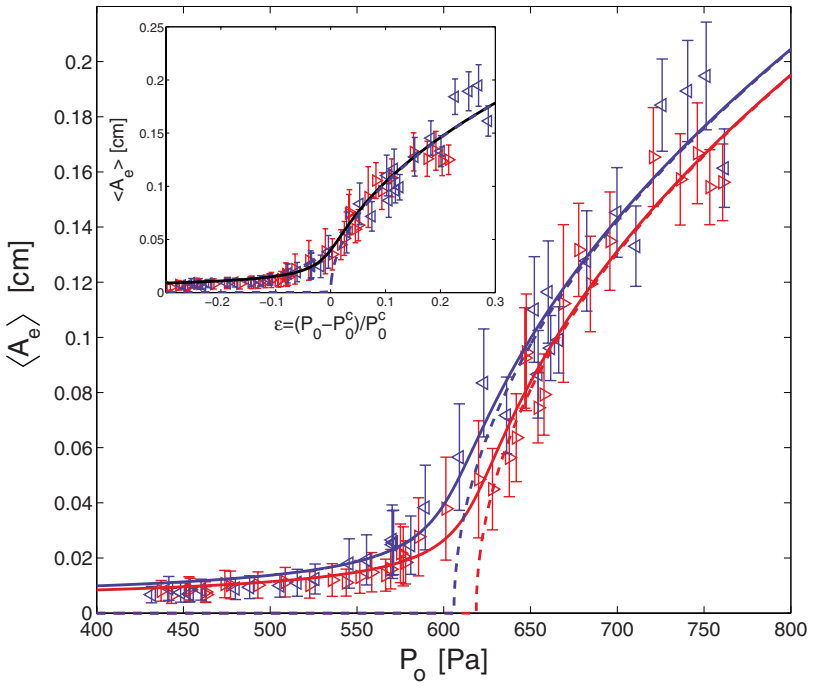

FIG. 5. (Color online) Main: bifurcation diagram of A_e for increasing ($\triangleright$) and decreasing ($\triangleleft$) values of P_o. Continuous lines are theoretical fits to a model that considers the effect of additive noise (see Sec. IV). For the increasing (decreasing) P_o ramp, the obtained parameters are the critical pressure $P_o^c = 619 \pm 15$ Pa ($P_o^c = 606 \pm 26$ Pa), the noise intensity $\eta = (3.9 \pm 2.1) \times 10^{-3}$ [$\eta = (5.1 \pm 3.5) \times 10^{-3}$], and the scale factor $\alpha_s = 0.36 \pm 0.05$ cm ($\alpha_s = 0.36 \pm 0.07$ cm). Dashed lines are the theoretical predictions $\langle A_e \rangle = \alpha_s [(P_o - P_o^c)/P_o^c]^{1/2}$ for increasing and decreasing ramps using the previous adjusted parameters. (Inset) Bifurcation diagram of A_e as a function of the reduced control parameter $\varepsilon = (P_o - P_o^c)/P_o^c$ for increasing ($\triangleright$) and decreasing ($\triangleleft$) ramps. Continuous line is the theoretical fit to a model that considers the effect of additive noise (see Sec. IV). Dashed line is the theoretical prediction $\langle A_e \rangle = \alpha_s \varepsilon^{1/2}$.

$\varepsilon=[(P_o-P_o^c)/P_o^c]^{1/2}$ is the reduced control parameter, but using the adjusted parameters with the theoretical prediction with noise. For the deterministic bifurcation, the parameters are the critical pressure P_o^c and the scale factor α_s. These curves fit quite well our data, but, as expected, only for a subset above the bifurcation point.

IV. THEORETICAL DESCRIPTION

To understand the formation process of the fluctuating subharmonic waves observed in the previously described experimental setup, we consider the use of amplitude equation techniques, bifurcation theory, and stochastic processes. This is a consequence of lack of a continuous or macroscopic description of granular flows, as we have mentioned before. Hence, our theoretical description is based on a universal description of the appearance of subharmonic standing waves.

Let us consider a forced one-dimensional extended system that exhibits a supercritical subharmonic standing-wave bifurcation which is described by the field $\vec{u}(x,t)$. This bifurcation accounts for the transition from a flat or uniform state $\vec{u}(x,t)=\vec{u}_0$ to a standing wave oscillating to the half of the forcing frequency f_o. Many pattern forming systems that are driven out of equilibrium exhibit traveling waves, standing waves, or alternating waves (periodic or even chaotic) [25,32]. Then, a natural description of these systems is to consider the dynamics of two counter propagating waves, which corresponds to the usual description in the Andronov-Hopf instability [25]. However, our parametrically driven system near resonance is characterized by exhibiting standing waves. Therefore, the central manifold (i.e., the minimal set of variables that describes the phenomena under study) that accounts for the stationary waves is attractive [30]. That is, if one considers as an initial condition a traveling wave, after a transient the system converges to a standing wave (see review [40]). Based on Floquet theory, the relation between the original variables and the critical mode is done by means of an asymptotic change of variable with periodic coefficients [31]. Hence, close to the bifurcation of our parametrically forced system, we consider the standing-wave central manifold. Thus, we present the following Ansatz for the subharmonic standing waves:

$$\vec{u}(x,t)=\vec{u}_0+(Ae^{ik_cx}+\bar{A}e^{-ik_cx})F(t)\hat{u}+\mathrm{HOT}, \tag{1}$$

where $A(x,t)$ stands for the complex envelop of subharmonic waves, $\hat{u}$ accounts for the critical mode, $F(t)$ is a periodic function of period $1/f_o$, and HOT are the higher-orders terms in the description of $\vec{u}(x,t)$. This means that the system is forced at f_o and it responds at $f_o/2$. We assume the system possesses a natural frequency f_n and that f_o is close to twice f_n. The difference between $2f_n$ and the forcing frequency is the called *detuning*.

Based on bifurcation theory, close to the bifurcation point, the envelope can be described as a slow spatiotemporal variable. The system under study is isotropic and homogeneous. Thus, the spatial translation symmetry $x\to x+x_0$ leads to a phase invariance symmetry for the envelope, $A\to Ae^{ik_cx_0}$. The spatial reflection symmetry $x\to -x$ leads to the conjugation symmetry for the envelope $A\to\bar{A}$. Therefore, using the above symmetries and the fact that the transition is supercritical the amplitude equation reads

$$\partial_t A=\varepsilon A-|A|^2A+\sqrt{\eta}\zeta(A;t), \tag{2}$$

where ε is the bifurcation parameter, $\zeta(A;t)$ accounts for random fluctuations of A, that is, it is a noise term and η is the noise level intensity. In this sense, Eq. (2) is simply a Ginzburg-Landau equation with real coefficients. It is important to note that in the unforced system—this means a system without parametric forcing—the appearance of standing or traveling waves, or even transitions between them, is not described appropriately by the above ansatz (1) because one needs to consider different amplitudes for the *left* and *right* traveling waves, that is $\vec{u}(x,t)=\vec{u}_0+a_+e^{i(k_cx-\omega t)}+a_-e^{-i(k_cx+\omega t)}+\cdots$ [21]. In this case, the system is described by two coupled Ginzburg-Landau equations (see [24,32] and references therein). In this framework, the unforced system close to the standing-wave transition is described by a Ginzburg-Landau equation [24]. This corresponds to Eq. (2) with complex coefficients.

A. Deterministic amplitude equation

In the deterministic case, $\eta=0$, for negative ε, the stable equilibrium is the zero amplitude state which represents a flat interface oscillating at the forcing frequency f_o. For positive ε, the model (2) exhibits a family of stable equilibrium states of the form $A=\sqrt{\varepsilon}e^{i\phi}$, where ϕ is an arbitrary constant related to the phase invariance of the pattern. For a given ϕ, this state accounts for the amplitude of the standing waves. Hence, A increases as $\sqrt{\varepsilon}$ and for $\varepsilon=0$ the model (2) exhibits a spatial bifurcation.

The stochastic term breaks all the mentioned symmetries of the envelope and is always present in the amplitude equation. This is due to the fact that this type of term cannot be removed using a change of variable, i.e., this is a resonant term (Appendix A of [33]). Close to the bifurcation point, the envelope is small, thus we can rewrite the stochastic term generically in the form

$$\zeta(A;t)=\sum_{n,m=1}\eta_{nm}A^n\bar{A}^m\zeta_{nm}(t), \tag{3}$$

where η_{nm} are constant parameters of order 1, $\zeta_{nm}(t)$ are stochastic terms modeled by Gaussian processes with zero mean value ($\langle\zeta_{nm}\rangle=0$), and correlation

$$\langle\zeta_{nm}(t)\zeta_{pq}(t')\rangle=\begin{cases}0, & n+p\neq m+q+2\\ \delta(t-t')C_{nmpq}, & n+p=m+q+2\end{cases} \tag{4}$$

and

$$\langle\zeta_{nm}(t)\bar{\zeta}_{pq}(t')\rangle=\begin{cases}0, & n+p\neq m+q\\ \delta(t-t')C_{nmpq}, & n+p=m+q,\end{cases} \tag{5}$$

where C_{nmpq} is the correlation matrix of the initial physical system, which characterizes the correlation between different constituent of the noise. The properties described above are a result of the change of variable from the physical variables to

the envelope ones. The noise term appearing in Eq. (2) is deduced from a spatial average of the noise of the primary physical model (see, for instance, [26]). When the noise is independent of amplitude A, is usually denominated *additive noise* [34]. Otherwise, it is termed *multiplicative noise*.

B. Amplitude equation with additive noise

As stated above, the amplitude of the standing wave is small close to the bifurcation. Thus, the fluctuations can be modeled by an additive noise and the amplitude equation reads as

$$\partial_t A = \varepsilon A - |A|^2 A + \sqrt{\eta}\zeta_{00}(t). \tag{6}$$

Note that the supercritical pattern formation in one-dimensional systems is described by the above stochastic equation [26]. Introducing the vectorial notation $\vec{q}=(A,\bar{A})$ and $\vec{\xi}=(\zeta_{00},\bar{\zeta}_{00})$, the above equation can be rewritten as

$$\partial_t q^\nu = -\varepsilon^{\nu\mu}\frac{\partial F}{\partial q^\mu} + \sqrt{\eta}\xi^\nu(t), \tag{7}$$

where $F \equiv -\varepsilon|A|^2+|A|^4/2$ is a Lyapunov potential, $\{\nu,\mu\}=1,2$ are indexes where there is sum over the repeated indexes, $\varepsilon^{\nu\mu}$ is an invertible symmetrical tensor defined as

$$\varepsilon^{\nu\mu} = \begin{cases} 0, & \nu=\mu \\ 1, & \nu\neq\mu, \end{cases} \tag{8}$$

and the autocorrelation function of $\xi^\mu(t)$ satisfies $\langle\xi^\nu(t)\xi^\mu(t')\rangle=\varepsilon^{\nu\mu}\delta(t-t')$. Hence, the dynamics of the deterministic model (6) is characterized by the minimization of F. The equation of the density probability function evolution of the complex amplitudes A and $\bar{A}$ $[P(A,\bar{A};t)]$ associated to the Langevin Eq. (6) is the Fokker-Planck equation that has the form [34]

$$\partial_t P = \frac{\partial}{\partial q^\nu}\left(\varepsilon^{\nu\mu}\frac{\partial F}{\partial q^\mu}P\right) + \eta\frac{\partial}{\partial q^\nu}\left(\varepsilon^{\nu\mu}\frac{\partial}{\partial q^\nu}P\right), \tag{9}$$

where the terms $\varepsilon^{\nu\mu}\frac{\partial F}{\partial q^\mu}$ and $\eta\varepsilon^{\nu\mu}$ are the drift and diffusion matrix of the density probability function. It is important to notice that given an initial distribution, it is a difficult task to find an analytical expression for probability density function as a function of time. However, in the stationary regime, it can be characterized by a simple expression. In the case of null flux boundary condition (which physically means that particles are not lost at the edges), it is trivial to show that the stationary density probability reads

$$P(A,A) = ce^{-F/\eta} = ce^{-[-2\varepsilon|A|^2+|A|^4]/2\eta}, \tag{10}$$

where c is a normalization constant and F is usually denominated *nonequilibrium potential* [35,36]. As mentioned above, experimentally we measure the envelope A_e of the critical mode A_c, which is, except a scale factor, equal to the modulus of the amplitude A. Introducing the modulus and phase variables $A=Re^{i\theta}$, we have $A_e=\alpha_s R$, where α_s is a scale factor. Thus, the above probability density reads

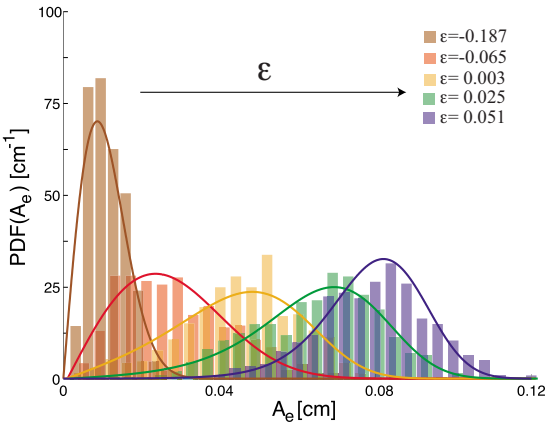

FIG. 6. (Color online) Computed histograms of A_e (bars) and theoretical generalized Rayleigh distribution (lines) [Eq. (11)] for increasing ε.

$$P(R,\varepsilon,\eta) = Q(\varepsilon,\eta)Re^{[2\varepsilon R^2-R^4]/2\eta} \tag{11}$$

after integrating on the phase variable, where the constant of normalization is

$$Q(\varepsilon,\eta) \equiv 2\sqrt{2}e^{-\varepsilon^2/2\eta}/\mathrm{erfc}(-\varepsilon/\sqrt{2\eta})\sqrt{\pi\eta}. \tag{12}$$

Below the bifurcation ($\varepsilon<0$) and neglecting the quartic term, the above probability density is the Rayleigh distribution [37], which describes the speed distribution of a bidimensional ideal gas. Hence, we have termed *generalized Rayleigh distribution* the distribution (11), which is valid below and above the subharmonic wave transition. This stationary probability density distribution is shown in Fig. 6 and compared to the experimental distribution for different values of the bifurcation parameter ε. The different colors bars in Fig. 6 stand for the normalized histogram obtained experimentally in the quasi-one-dimensional fluidized shallow granular bed close to subharmonic wave transition. It should be noticed that another generalization of the Rayleigh distribution has been obtained in oscillatory instabilities with linear multiplicative noise [20,21].

The probability density distribution (11) is an asymmetrical function with respect to its maximum. Thus, as shown in Ref. [26], the most relevant quantity for characterizing $P(R,\varepsilon,\eta)$ is its most probable value and not its mean value. The value of $R_{\max}$ corresponding to the maximum of $P(R,\varepsilon,\eta)$ occurs at

$$R_{\max} = \sqrt{\frac{\varepsilon+\sqrt{\varepsilon^2+2\eta}}{2}}. \tag{13}$$

The average of R can also be computed but its analytical form is much more complex. The simplicity of this expression allows a direct interpretation of its parameters and, as it will be shown later, is a fairly good approximation to the average value of R. For large positive ε, the expression (13) for the most probable value can be accurately approached by $R_{\max}\approx\sqrt{\varepsilon}$. Hence, the amplitude of the subhamonic waves increases with the square root of bifurcation parameter ε. For negative ε, the most probability value is approached by

$R_{\max} \approx \sqrt{\eta/2|\varepsilon|}$, that is, the amplitude of the precursor of the standing wave is proportional to square root of noise level intensity and inversely proportional to the bifurcation parameter. Figure 5 shows the experimental mean value for A_e in our quasi-one-dimensional fluidized shallow granular bed close to subharmonic wave transition and its comparison to the theoretical expression (13). More precisely, defining the experimental control parameter $\epsilon=(P_o-P_o^c)/P_o^c$, the continuous curves in Fig. 5 are fits of the form

$$\langle A_e \rangle = \alpha_s \sqrt{\frac{\epsilon + \sqrt{\epsilon^2 + 2\eta}}{2}}, \tag{14}$$

where P_o^c is the critical P_o and η is the noise intensity. Here, the fitting parameters are P_o^c, η, and the scale factor α_s. For our experimental setup, the value of noise intensity is $\eta \approx 5 \times 10^{-3}$, which is within the experimental and numerical ranges already reported in [17,22]. As already stated in [22], this noise intensity is almost 1 order of magnitude larger than the largest noise strength obtained in experiments in ordinary fluids near the critical point, while values typical for convection are closer to 10^{-9} [38].

The generalized Rayleigh distribution possesses only one maximum. Below the bifurcation point, the maximum of the distribution is reached for a small value of $R_{\max}$. As the bifurcation parameter is increased, the maximum of the distribution decreases and $R_{\max}$ moves to larger values (cf. Fig. 6). Increasing the bifurcation parameter up to the critical value $\varepsilon_c \equiv \sqrt{\eta/32}$ [26], the maximum of the distribution continues systematically to decrease, while $R_{\max}$ moves further to a larger values. Note that this behavior of probability density function even occurs for values above the bifurcation point $(0 < \varepsilon \leq \varepsilon_c)$. Increasing further the bifurcation parameter, the maximum moves to larger values, however, the maximum systematically increases with the bifurcation parameter as is illustrated in Fig. 6. Hence, a bigger dispersion of the system—that is, the system is more noisy—is expected close to the transition at $\varepsilon = \varepsilon_c$. The probability density distribution shown in Fig. 6 depicts the above scenarios close to the bifurcation.

However, for even larger values of the bifurcation parameter, the experimental normalized histograms change their behavior. Namely, the maximum of probability density function decreases when the pressure amplitude P_o is increased. Ultimately, it increases again. Figure 7 illustrates this behavior. Therefore, the generalized Rayleigh distribution formula (11) only describes the probability density distribution close to subharmonic wave transition of forced systems. For larger distances to the bifurcation point, additive noise is not enough to explain the experimentally observed behavior.

C. Amplitude equation with multiplicative noise

To understand the density distribution function far from the transition point, we must to take into account in the theoretical description the amplitude dependence of noise—multiplicative noise. For the sake of the simplicity, we can approach the multiplicative noise term by

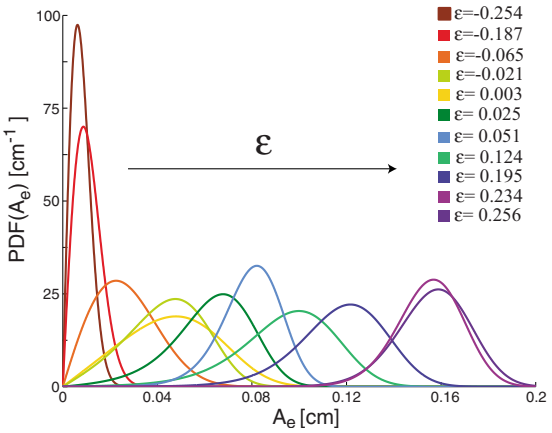

FIG. 7. (Color online) Theoretical interpolations of the probability density distributions obtained from the experimental normalized histograms of the amplitude fluctuations for increasing ε.

$$\zeta(A;t) \approx \zeta_{00}(t) + \alpha A \zeta_{10}(t) + \beta \bar{A} \zeta_{01}(t), \tag{15}$$

where α and β are arbitrary coefficients. $\zeta_{00}(t)$, $\zeta_{10}(t)$, and $\zeta_{01}(t)$ have zero mean values and are delta-correlated following Eq. (5). Hence, all noise terms are independent. Using the vectorial notation of the previous section, the amplitude equation reads

$$\partial_t q^\nu = -\varepsilon^{\nu\mu} \frac{\partial F}{\partial q^\nu} + \sqrt{\eta}[\xi^\nu(t) + \kappa^\nu(q^\mu, t)], \tag{16}$$

where the extra multiplicative noise terms are $\vec{\kappa} \equiv [\alpha A \zeta_{10}(t) + \beta \bar{A} \zeta_{01}(t), \alpha \bar{A} \bar{\zeta}_{10}(t) + \beta A \bar{\zeta}_{01}(t)]$.

Analogously to the model represented by Eq. (6), the deterministic dynamics of the new model is characterized by the minimization of the Lyapunov function F. The equation of the density probability distribution now reads [34]

$$\partial_t P = \frac{\partial}{\partial q^\nu}\left(\varepsilon^{\nu\mu} \frac{\partial F}{\partial q^\mu} P\right) + \eta \frac{\partial}{\partial q^\nu}\left(\varepsilon^{\nu\mu} \frac{\partial}{\partial q^\mu} P\right) + \eta \frac{\partial}{\partial q^\nu}\left(\varepsilon^{\nu\mu} \gamma |A|^2 \frac{\partial}{\partial q^\mu} P\right), \tag{17}$$

where $\gamma \equiv \alpha^2 + \beta^2$. The second line is directly the corrective term associated to the effect of the simple multiplicative term we have added to our model. To characterize the stationary regime and considering that close to the bifurcation the amplitude A is small, then we assume $\gamma |A|^2 \ll 1$. Hence, the last term of Eq. (17) can be considered as a perturbation. Then, the stationary probability satisfies

$$\frac{1}{\eta[1 + \gamma |A|^2]} \frac{\partial F}{\partial q^\mu} = -\frac{1}{P} \frac{\partial}{\partial q^\mu} P.$$

Expanding the left-hand side in γ series and considering the ansatz for the probability $P = c e^{-(F+\Theta)/\eta}$, where $\Theta \ll 1$, we obtain after straightforward calculations

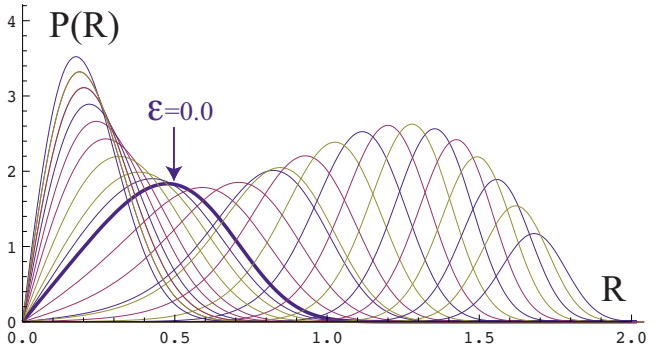

FIG. 8. (Color online) Theoretical probability density distributions formula (20) as function of bifurcation parameter with $\eta=0.1$ and $\gamma=0.2$. ε increases to the right with a step of 0.2. Arrow shows the curve for $\varepsilon=0.0$.

$$\frac{\partial\Theta}{\partial q^{\mu}} \approx -[\gamma|A|^2 + \gamma^2|A|^4]\frac{\partial}{\partial q^{\mu}}F. \tag{18}$$

Introducing the expression of the Lyapunov function and integrating, we find

$$\Theta \approx \gamma\left(\varepsilon\frac{|A|^4}{2} - \frac{|A|^6}{3}\right) - \gamma^2\left(\varepsilon\frac{|A|^6}{3} - \frac{|A|^8}{4}\right). \tag{19}$$

Hence, the density probability distribution for the amplitude modulus for multiplicative noise takes the form

$$P(R,\varepsilon,\eta) \approx cRe^{[\varepsilon R^2 - R^4/2 - \gamma(\varepsilon(R^4/2) - R^6/3) + \gamma^2(\varepsilon(R^6/3) - R^8/4)]/\eta}. \tag{20}$$

This probability density distribution has qualitatively the same form of the generalized Rayleigh distribution (11). Nevertheless, the behavior of its maximum as a function of the bifurcation parameter changes. As the bifurcation parameter moves further away from the bifurcation point, the maximum initially increases and later decreases, as it is shown in Fig. 8. Experimentally, we observe qualitatively the same evolution of probability density distribution. This is a signature of the effect of multiplicative noise in the system under study. To accurately describe this behavior, a quantitative description requires higher-order terms in the drift and the noise terms. Another strategy to study theoretically the probability density distribution is to consider the weak noise limit ($\eta\to 0$), where the nonequilibrium potential can be written as polynomial expansion in the amplitude [36]. Nevertheless, given that the system under study is composed by a few constituents (in comparison to Avogadro's number, for instance), the intensity of the noise, which is related to the fluctuations of the internal degrees of freedom of the granular layer, is not small at all. Hence, the strategy described above does not apply. Experimentally, we have compared the amplitude modulus of the subharmonic standing waves to the simple expression for the most probable value [Eq. (13)] as it is depicted in Fig. 5. Figure 9 shows the mean value obtained with the probability density distribution of the modulus for additive and multiplicative noises, which are indistinguishable. In this figure, we also present a comparison of the mean and most probable values, following formula (13), where one can conclude that the most probable value is an adequate statistical quantity [26].

V. CONCLUSIONS AND COMMENTS

Fluidized granular matter lacks of a well-established macroscopic continuum description, mainly due to the large inherent fluctuations which granular matter display. However, it exhibits similar dynamical behaviors as do everyday fluids. An example of this fact is the appearance of surface waves. Here, we show that the pattern formation process of standing fluctuating subharmonic waves on a fluidized quasi-one-dimensional shallow granular bed can be understood in terms of a universal theory of dynamical systems. This approach succeeds in describing qualitatively, through the use of amplitude equations, bifurcation theory, and stochastic processes, the growth of the critical mode of the pattern in a fluctuating medium, such as a fluidized shallow granular layer. Measurements of the amplitude of the critical mode of the fluctuating subharmonic waves close to the transition are in quite good agreement with those inferred from a universal stochastic amplitude equation. This allows us to determine the bifurcation point, the noise intensity, and, even, to characterize the appearance of precursors to the surface wave

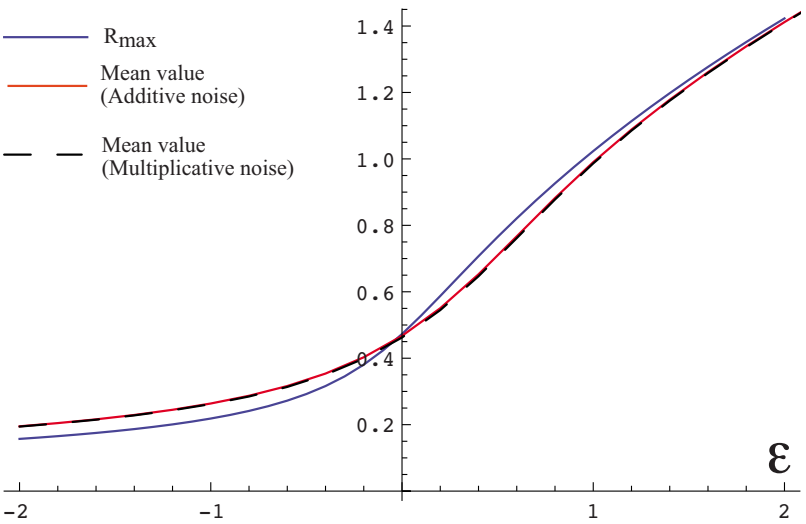

FIG. 9. (Color online) Mean values and most probable value as functions of bifurcation parameter with $\eta=0.1$ and $\gamma=0.2$. The continuous dark, light, and dashed curves, respectively, are the most probable formula (13) and mean values obtaining from the probability density distribution in the additive and the multiplicative noises.

pattern. Therefore, close to the spatial instability, the most appropriate and simplest theoretical description to compare experimental results is the amplitude equation given by Eq. (2).

We study also the statistical properties of the amplitude fluctuations of the pattern. For the stationary state observed experimentally, we show that probability density distribution is well described by a generalized Rayleigh distribution, which we compute directly as the stationary solution of the Fokker-Planck equation of the amplitude fluctuating evolution. In addition, we present a theoretical description of the behavior of the amplitude fluctuations far from the bifurcation point. The large amplitude fluctuations which are observed experimentally are attributed to the multiplicative nature of noise in our system under study. Further questions remain to be answered, which are related directly to the mechanism of the instability in air-mediated fluidization. For instance, subcritical behavior of the pattern amplitude has been observed in preliminary experiments [29]. Experimental and theoretical studies are currently being performed in this direction.

The presented theoretical description is universal. A simplified form was indeed used to model the experimental data obtained in a liquid crystal system [26]. It should also be applicable to other systems that present bifurcations in noisy environments, such as in a vibrated granular layer that undergoes a subharmonic wave transition [17] and for the oscillatory instability of magnetic grains in a turbulent flow [39]. In fact, the latter work presents bifurcation diagrams that resemble those presented here.

ACKNOWLEDGMENTS

The authors would like to thank to S. Rica and specially C. Orellana for fruitful discussions of the preliminary results of this study. M.G.C., N.M., and C.F. acknowledge the financial support of FONDECYT Grant Nos. 1090045, 1090188, and 11090049, respectively. M.G.C. and N.M. acknowledge the financial support of FONDAP Grant No. 11980002. C.F. acknowledges the financial support of Facultad de Ciencias Físicas y Matemáticas, Universidad de Chile.

[1] H. M. Jaeger, S. R. Nagel, and R. P. Behringer, Rev. Mod. Phys. **68**, 1259 (1996).
[2] I. S. Aranson and L. S. Tsimring, Rev. Mod. Phys. **78**, 641 (2006).
[3] J. Duran, *Sands and Powders, and Grains: An Introduction of the Physics of Granular Materials* (Springer, New York, 2000).
[4] D. Geldart, *Gas Fluidization Technology* (Wiley, New York, 1986).
[5] L. S. Tsimring, R. Ramaswamy, and P. Sherman, Phys. Rev. E **60**, 7126 (1999).
[6] J. Duran, Phys. Rev. Lett. **84**, 5126 (2000); **87**, 254301 (2001).
[7] J. Li, I. S. Aranson, W. K. Kwok, and L. S. Tsimring, Phys. Rev. Lett. **90**, 134301 (2003).
[8] J. T. Jenkins and M. W. Richman, Arch. Ration. Mech. Anal **87**, 355 (1985).
[9] J. T. Jenkins and M. W. Richman, J. Fluid Mech. **192**, 313 (1988).
[10] J. J. Brey, F. Moreno, and J. W. Dufty, Phys. Rev. E **54**, 445 (1996).
[11] N. Sela, I. Goldhirsch, and S. H. Noskowicz, Phys. Fluids **8**, 2337 (1996).
[12] J. J. Brey, J. W. Dufty, C. S. Kim, and A. Santos, Phys. Rev. E **58**, 4638 (1998).
[13] E. L. Grossman, T. Zhou, and E. Ben-Naim, Phys. Rev. E **55**, 4200 (1997).
[14] V. Garzó and J. W. Dufty, Phys. Rev. E **59**, 5895 (1999).
[15] D. Risso and P. Cordero, Phys. Rev. E **65**, 021304 (2002).
[16] C. Cartes, M. G. Clerc, and R. Soto, Phys. Rev. E **70**, 031302 (2004).
[17] D. I. Goldman, J. B. Swift, and H. L. Swinney, Phys. Rev. Lett. **92**, 174302 (2004).
[18] J. Swift and P. C. Hohenberg, Phys. Rev. A **15**, 319 (1977); P. C. Hohenberg and J. B. Swift, *ibid.* **46**, 4773 (1992).
[19] J. Garcia-Ojalvo and J. M. Sancho, *Noise in Spatially Extended Systems* (Springer-Verlag, New York, 1999).
[20] R. Graham, Phys. Rev. A **25**, 3234 (1982).
[21] F. Drolet and J. Vinals, Phys. Rev. E **56**, 2649 (1997).
[22] J. Bougie, J. Kreft, J. B. Swift, and H. L. Swinney, Phys. Rev. E **71**, 021301 (2005).
[23] G. Nicolis and I. Prigogine, *Self-Organization in Non Equilibrium Systems* (J.Wiley & Sons, New York, 1977).
[24] L. M. Pismen, *Patterns and Interfaces in Dissipative Dynamics*, Springer Series in Synergetics (Springer, Berlin, 2006).
[25] M. Cross and H. Greenside, *Pattern Formation and Dynamics in Nonequilibrium Systems* (Cambridge University Press, New York, 2009).
[26] G. Agez, M. G. Clerc, and E. Louvergneaux, Phys. Rev. E **77**, 026218 (2008).
[27] W. Schöpf and W. Zimmermann, Phys. Rev. E **47**, 1739 (1993).
[28] M. Faraday, Philos. Trans. R. Soc. London **52**, 319 (1831).
[29] C. Orellana, M.S. thesis, Universidad de Chile, 2005.
[30] G. Iooss and M. Adelmeyer, *Topics in Bifurcation Theory and Applications* (World Scientific, Singapore, 1998).
[31] V. I. Arnold, *Geometrical Methods in the Theory of Ordinary Differential Equations* (Springer-Verlag, New York, 1983).
[32] M. Clerc and P. Coullet, Phys. Rev. E **60**, 6589 (1999).
[33] M. G. Clerc, C. Falcon, and E. Tirapegui, Phys. Rev. E **74**, 011303 (2006).
[34] N. G. Van Kampen, *Stochastic Process in Physics and Chemistry* (North-Holland, Amsterdam, 1992).
[35] R. Graham and T. Tel, Phys. Rev. A **33**, 1322 (1986).
[36] O. Descalzi and E. Tirapegui, J. Stat. Phys. **57**, 993 (1989).
[37] A. Papoulis, *Probability, Random Variables, and Stochastic Processes* (McGraw-Hill, New York, 1984).
[38] J. Oh and G. Ahlers, Phys. Rev. Lett. **91**, 094501 (2003).
[39] B. Gallet and F. Pétrélis, Europhys. Lett. **87**, 54004 (2009).
[40] M. C. Cross and P. C. Hohenberg, Rev. Mod. Phys. **65**, 851 (1993).